

Tunable immunonanoparticle binding to cancer cells: thermodynamic analysis of targeted drug delivery vehicles†

Karyn Ho,^{ab} Yakov Lapitsky,^a Meng Shi^{ab} and Molly S. Shoichet^{*abcd}

Received 15th August 2008, Accepted 27th November 2008

First published as an Advance Article on the web 29th January 2009

DOI: 10.1039/b814204a

Tumour cells are often associated with altered surface receptor profiles, and these changes can provide a basis for targeted delivery of anti-cancer agents. Functionalizing a colloidal drug delivery vehicle, such as a polymeric nanoparticle, with several targeting ligands has qualitatively been shown to increase the effective affinity of the nanoparticle for its target receptor over the affinity of the free ligand. However, whether this increase results from multiple simultaneous interactions per particle (multivalent binding) or increased configurations for single binding events per particle (monovalent binding) is unclear. A quantitative approach was required to distinguish between these possible mechanisms. In this study, human epidermal growth factor receptor 2 (HER2) overexpressing cancer cells (SKBR-3) were used as the target for anti-HER2 (trastuzumab, HerceptinTM) immunonanoparticles. We varied the antibody conjugation density on the immunonanoparticles and measured their cellular binding by a flow cytometric immunoassay. Using this method, we were able to directly assay the targeted cells and quantify immunonanoparticle binding strength, allowing us to better understand whether immunonanoparticles were bound by monovalent or multivalent interactions. The binding data for each formulation were fitted to Langmuir isotherms, and based on the theory presented herein, it was concluded that the system studied behaved in a manner consistent with monovalent binding. Understanding this property of immunonanoparticle binding is useful in drug delivery applications, where manipulating the strength of such interactions is essential to controlling their targeting capacity on both tissue and cellular levels. The models developed here can be used to quantitatively predict binding strength for rational immunonanoparticle design.

Introduction

The development of targeted drug carriers is driven by limitations identified with the free administration of anti-cancer agents, including short plasma half lives, systemic toxicity, and mass transport barriers restricting accumulation at tumour sites.^{1–4} The altered phenotype of cancer cells often includes changes to their surface receptor profiles, providing a basis for active targeting using monoclonal antibodies that recognize and bind specific receptors with elevated expression levels.^{1,5,6} Covalent attachment of such antibodies to polymeric drug carriers allows their guided transport to the surfaces of targeted cells, while the polymer is designed to protect drug bioactivity, increase circulation time,

and shield healthy cells from cytotoxic agents.^{2–4,7,8} Moreover, binding can enhance retention at tumour sites and can introduce a means for rapid receptor-mediated internalization of drug-loaded carriers into the intracellular compartment, a common site of action for cytotoxic drugs.^{2,4,9,10}

In the case of colloidal drug-loaded polymer aggregates, including self-assembled polymeric nanoparticles, every polymer chain can participate in drug delivery, but the direct modification of each polymer chain with a targeting antibody becomes unnecessary; unmodified polymer chains can be targeted as members of a modified aggregate, and fewer targeting antibodies are then required overall.¹¹ The number of antibodies per aggregate can be controlled by varying the reaction conditions during their attachment (*e.g.*, reaction time, feed ratio of antibody to polymer).⁶ Enhanced binding strength of immunonanoparticles over free antibody can occur through two possible mechanisms: the introduction of multiple simultaneous interactions per particle (multivalent binding, see Fig. 1A) or the increase in possible configurations for single binding events per particle (monovalent binding, see Fig. 1B).

Multivalent binding events would greatly enhance binding through avidity, where the presentation of multiple tethers to the cell surface maintains association and cell-particle proximity after a single dissociation event, thereby promoting re-attachment.¹² A more moderate increase in binding strength is associated with monovalent binding.¹³ The dramatic increase in binding strength associated with avidity is a phenomenon that

^aDepartment of Chemical Engineering & Applied Chemistry, University of Toronto, 200 College Street, Toronto, ON, Canada M5S 3E5. E-mail: dept.chemeng@utoronto.ca; Fax: +416-978-8605; Tel: +416-978-3063

^bInstitute of Biomaterials & Biomedical Engineering, University of Toronto, 407-164 College Street, Toronto, ON, Canada M5S 3G9; Fax: +416-978-4317

^cDepartment of Chemistry, University of Toronto, 80 St. George Street, Toronto, ON, Canada M5S 3H6; Fax: +416-978-8775; Tel: +416-978-3564

^dUniversity of Toronto, 514-160 College Street, Toronto, ON, Canada M5S 3E1. E-mail: molly.shoichet@utoronto.ca; Fax: (+416) 978-4317; Tel: (+416) 978-1460

† Electronic supplementary information (ESI) available: Schematic illustration of available combinations for monovalent binding. See DOI: 10.1039/b814204a

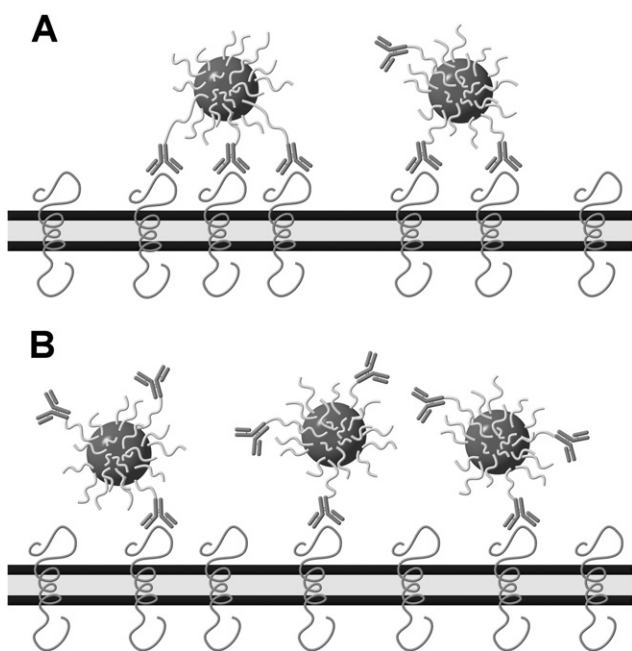


Fig. 1 Functionalizing immunonanoparticles with greater numbers of targeting antibodies enhances their ability to associate with target cells. This effect can result from (A) increases in binding events per particle (multivalent binding) or (B) increases in possible binding configurations with a single interaction (monovalent binding). Illustrated here are immunonanoparticles with $\Omega = 3$ attached antibodies. In (A), the number of antibodies bound to cell receptors, α , is shown as $\alpha = 3$ (left) and $\alpha = 2$ (right). In (B) the number of antibodies bound to cell receptors, α , is shown as $\alpha = 1$ for all nanoparticles. The mechanism is an important consideration in immunonanoparticle design, as it dictates how binding strength will increase as the antibody conjugation density increases.

would be most beneficial for antibodies that have poor affinity with their targets.^{8,14,15} Conversely, in cases where the binding affinity is very high, there is decreased utility in treating solid tumours, where complete tumour penetration can be limited by strong association with cells directly adjacent to tumour vasculature.^{7,16,17} Heterogeneity of targeting within the tumour mass leads to incomplete eradication of tumour cells, as certain cells will receive either no drug or levels of drug below the therapeutic index.¹⁶ Furthermore, binding strength influences the cell-associated fraction at a given particle concentration, and this information helps assess whether the particle dosage administered delivers drug levels within the therapeutic index.¹⁸

Whether multivalent interactions can occur is predicated on both the density of the targeted receptor on the cell surface and the density of binding sites on the drug carrier. Quantitative avidity measurements have been performed using receptors immobilized onto a hard synthetic substrate.^{19–21} However, interactions with cells can be dramatically different, in part because lateral movement of receptors within the cell membrane can result in transient increases in local receptor density; this phenomenon has previously been shown with solutions of free antibody.²² Having a flexible polymeric spacer, such as poly(ethylene glycol) (PEG), between the nanoparticle core and the targeting molecule, provides the latter with greater free volume (and thus greater likelihood) to interact with cellular receptors.²³

A simple, quantitative method to investigate the binding interactions between cells and immunonanoparticles by directly assaying the targeted cells is lacking. We developed a flow cytometric immunoassay to assess equilibrium cell binding of an anti-human epidermal growth factor receptor 2 (anti-HER2) immunonanoparticle system. HER2 is a cell surface receptor that becomes overexpressed in 20–30% of breast cancer cases. It is used as an indication for treatment with Herceptin (trastuzumab),^{24–27} which is the anti-HER2 monoclonal antibody conjugated to the polymeric nanoparticles in this study. SKBR-3 cells were chosen as an *in vitro* model of HER2 overexpression, and express 1×10^6 receptors/cell,²⁸ using this model, we have shown previously that the binding of Herceptin-immunonanoparticles is receptor specific, with little non-specific adsorption.⁶ Here we varied the number of conjugated antibodies per nanoparticle, measured dose responsive binding, and, by fitting binding isotherms to each, quantified how the cell-particle binding varies with the density of conjugated antibodies. Thermodynamic analysis of these variations elucidates the nature of the binding events between our anti-HER2 immunonanoparticles and HER2 overexpressing SKBR-3 cells in culture. This reveals a linear scaling between the immunonanoparticle binding strength and the number of conjugated antibodies, thereby providing quantitative guidelines for tuning cell-particle interactions in the design of colloidal vehicles for targeted drug delivery.

Experimental

Materials

All cell culture materials were purchased from Gibco-Invitrogen (Burlington, ON, Canada). SKBR-3 cells were obtained through ATCC (Manassas, VA, USA). Dialysis membranes were acquired from Spectrum Laboratories (Rancho Dominguez, CA, USA). The Herceptin antibody was purchased through Hoffmann-La Roche Limited (Mississauga, ON, Canada). The polymeric nanoparticles were synthesized as previously described.^{6,29} All other materials were purchased from Sigma-Aldrich (Mississauga, ON, Canada) and used as received unless otherwise noted.

Nanoparticle synthesis

An aqueous suspension of poly(2-methyl-2-carboxytrimethylene carbonate-*co-D,L*-lactide)-*graft*-poly(ethylene glycol)-furan (poly(TMCC-*co*-LA)-*g*-PEG-furan) nanoparticles was prepared by dialysis, as reported previously.^{6,29} Briefly, the polymer was first dissolved in a mixture of 95 vol% dimethylformamide (DMF) and 5 vol% 500 mM borate buffer, pH 9.0 at a final concentration of 10 mg/mL; the solution was then dialysed a minimum of four times against distilled water at room temperature over 24 h using a 12–14 kDa molecular weight cut off membrane. This procedure yielded nanoparticles with a mean hydrodynamic diameter of 80 nm as measured by dynamic light scattering (Brookhaven 90Plus Particle Sizer, Brookhaven Instruments, Holtsville, NY, USA) with the hydrophobic poly(TMCC-*co*-LA) backbone comprising the nanoparticle core, and the hydrophilic, flexible, furan-terminated PEG grafts comprising the nanoparticle shell. Site-specific chemical modification of carbohydrates on the Fc region of the Herceptin antibody provided a maleimide functional

group, allowing covalent attachment of Herceptin to the PEG-furan termini through Diels–Alder chemistry.^{6,29} Specifically, a furan-functionalized nanoparticle solution (4 mg in 1 mL of distilled water) was mixed with maleimide modified Herceptin (100 µg in 120 µL of 100 mM β-morpholinoethanesulfonic acid (MES) buffer, pH 5.5) and incubated at 37 °C. By adjusting the reaction time (20 min, 1, 2, and 4 h), the antibody conjugation density was varied to have an average of 1.9 ± 0.3 , 3.2 ± 0.5 , 5.9 ± 0.2 , and 9.4 ± 0.9 antibodies/nanoparticle, based on a 95% confidence interval. The average values were estimated as previously reported, based on the hydrodynamic particle diameter, by comparing the fluorescence intensity of the Alexa Fluor® 430-labelled Herceptin and immunonanoparticles made by reaction with this fluorescent Herceptin.⁶ The resulting immunonanoparticles were then purified using a Sephacryl S-300HR column equilibrated in phosphate buffered saline, pH 7.4 (PBS).

Cell lines and maintenance

SKBR-3 cells were maintained in McCoy's 5A culture medium, supplemented with 10% heat-inactivated fetal bovine serum (FBS), 50 units/mL penicillin and 50 µg/mL streptomycin under a humidified 5% CO₂ environment. To prepare cell suspensions, adherent cells were first rinsed with PBS, then incubated briefly with trypsin-ethylenediamine tetraacetic acid (trypsin-EDTA, 0.25%/0.038%). Once the cells were suspended, enzymatic digestion was inhibited with FBS, and the cells were pelleted and resuspended at the desired concentration.

Flow cytometric analysis

To quantify immunonanoparticle binding, a fluorescently labeled secondary antibody was used for detection. Subsequent intensity measurements could then be carried out on a cell by cell basis by fluorescence activated cell sorting (FACS), where the intensity values are proportional to the number of bound immunonanoparticles. To do this, SKBR-3 cells were first suspended, as described above, in PBS at a final concentration of 1×10^6 cells/mL and distributed into 200 µL aliquots in 1.7 mL centrifuge tubes. The cells were then incubated for 30 min at 4 °C to inhibit endocytosis (cellular uptake), and resuspended in 200 µL of immunonanoparticle solution at varying concentrations in triplicate. The cells were again incubated for 30 min at 4 °C to reach equilibrium binding,^{22,30,31} and washed with 1 mL of cold PBS, pelleted, and resuspended in 50 µL of FACS buffer (PBS supplemented with 1% FBS and 2 mM EDTA). Rabbit anti-human immunoglobulin G-fluorescein isothiocyanate (IgG-FITC) secondary antibody was diluted 1/200 in PBS, and 10 µL was added to each of the cell suspensions. After 30 min incubation at 4 °C, the cells were washed with 1 mL cold FACS buffer, resuspended in 550 µL of fresh FACS buffer with 0.6 µg/mL propidium iodide (PI), and transferred to 5 mL FACS tube for analysis. Data acquisition was performed on a FACS Calibur (Becton Dickinson, Mississauga, ON, Canada) and analysis was performed using CellQuest software (Becton Dickinson). The first 10,000 events were recorded, and the live cell population was gated for analysis of FITC fluorescence intensity. All values shown are the average of triplicate samples with error bars representing their standard deviation.

Theory

As a first order approximation, the binding of polymeric immunonanoparticles (diameter ~ 100 nm) to much larger cancer cells (diameter ~ 10 µm) can be quantified using the Langmuir binding isotherm, where the binding strength is quantified using a single equilibrium binding constant, K_{eq} :

$$\theta = \frac{K_{eq}C_{NP}}{1 + K_{eq}C_{NP}} \quad (1)$$

Here, θ represents the fraction of the occupied binding surface on the cell and C_{NP} is the solution nanoparticle concentration. The number of spaces available for nanoparticle binding is dependent on the density of the targeted receptor, and in the case of very high receptor expression levels, is sterically limited by the volumes occupied by bound nanoparticles.³² The available potential binding space can be further limited in cases where receptor clustering occurs. Indeed, cancer cells with varying levels of receptor overexpression have previously been shown to have similar saturation concentrations, likely because further binding is sterically hindered.¹⁸ The isotherm accounts for these variations by defining θ as a fraction of saturation, the upper limits of which are influenced by receptor density and distribution, as well as particle size.

The binding constant, K_{eq} (which is often also reported as its reciprocal, the dissociation constant, K_d), is related to the molar Gibbs free energy of binding ($\Delta\bar{G}$) via:

$$K_{eq} = \exp\left(-\frac{\Delta\bar{G}}{RT}\right) \quad (2)$$

The variations in K_{eq} and $\Delta\bar{G}$ with the number of antibodies on the nanoparticle surface is influenced by two primary effects: (1) multivalent cell-nanoparticle interactions (avidity) and (2) an increase in the number of possible monovalent binding configurations for a single cell-nanoparticle pair. The thermodynamic analysis of these two mechanisms is outlined below.

Multivalent binding

Multivalent binding enhances binding stability by establishing multiple tethers to the binding surface; when a single interaction is disrupted, the remaining interactions maintain cell-particle proximity, thereby promoting subsequent re-attachment. In the case where the number of antibodies on the nanoparticle surface, Ω , affects the valency of the cell-particle interaction (see Fig. 1A), the molar Gibbs free energy of nanoparticle binding is roughly proportional to the average number of antigen-antibody interactions, α :³³

$$\Delta\bar{G}(\Omega) \sim \alpha\Delta\bar{G}(1) \quad (3)$$

Where $\Delta\bar{G}(\Omega)$ is the molar Gibbs free energy of the α -valent antibody-antigen binding and $\Delta\bar{G}(1)$ is the molar Gibbs free energy of binding for a single antigen-antibody pair. This linearity reflects the additivity of the antigen-antibody interactions. However, deviations from this relationship can exist due to cooperative and anti-cooperative interactions between the coupled antigen-antibody pairs.³³ Combining this result with

Equation 2 indicates an exponential dependence between K_{eq} and the number of interacting nanoparticles:

$$K_{eq}(\Omega) \sim K_{eq}(1)^\alpha \quad (4)$$

Thus, multivalent interactions can result in an increase of several orders of magnitude in the immunonanoparticle binding strength as the number of conjugated antibodies is increased, with α being a function of Ω . In the event of infrequent multivalent interactions ($1 < \alpha < 2$), this increase will be less dramatic, but the value for K_{eq} should increase exponentially.

Monovalent binding

In contrast to multivalent binding, for monovalent interaction, the amplified binding affinity may reflect an increase in the number of unique configurations for a single nanoparticle with Ω conjugated antibodies to bind to the cell surface (see Fig. 1B). In this case, the binding strength can be approximated theoretically by defining a canonical partition function, $Q(M, N, T)$, for N nanoparticles binding to M binding sites:³⁴

$$Q(N, M, T) = \Omega^N \times \frac{M!}{N!(M-N)!} \times \exp\left(\frac{-\varepsilon N}{k_B T}\right) \quad (5)$$

where the first term accounts for the internal degrees of freedom of N nanoparticles bound to the cells, the second term accounts for the number of lattice configurations in which these particles bind to M sites, and the third term is the Boltzmann factor for N nanoparticles binding to the cells with the molecular energy, ε (see Fig. S1 in ESI†).

The chemical potential of the cell-bound nanoparticles (μ_A) can be calculated using the following relationship:³⁴

$$\mu_A = -k_B T \left(\frac{\partial \ln Q(N, M, T)}{\partial N} \right)_{M, T} \quad (6)$$

This yields the expression:

$$\mu_A = \varepsilon - k_B T \ln \Omega + k_B T \ln \left(\frac{\theta}{1-\theta} \right) \quad (7)$$

where θ is equal to N/M . Because at equilibrium this chemical potential is equal to the chemical potential of the nanoparticles in solution (*i.e.*, $\mu_S = \mu_{S,0} + k_B T \ln C_{NP}$), θ can be solved as a function of the free nanoparticles in solution, C_{NP} :

$$\theta = \frac{K_{eq}(\Omega) C_{NP}}{1 + K_{eq}(\Omega) C_{NP}} \quad (8a)$$

where

$$K_{eq}(\Omega) = \Omega \exp\left(\frac{\mu_{d,0} - \varepsilon}{k_B T}\right) \quad (8b)$$

From these, expressions for variations in K_{eq} and $\Delta\bar{G}$ with Ω are obtained as:

$$K_{eq}(\Omega) = \Omega K_{eq}(1) \quad (9)$$

$$\Delta\bar{G}(\Omega) = \Delta\bar{G}(1) - RT \ln \Omega \quad (10)$$

Thus, in the absence of multivalent interactions (and the presence of monovalent interactions), K_{eq} is predicted to increase linearly with Ω , and $\Delta\bar{G}$ to vary logarithmically through the proportionality constant, RT .

Results and discussion

Over the range of Herceptin and nanoparticle concentrations studied, Herceptin immunonanoparticles (bearing between 1.9 and 9.4 antibodies per particle) bound to the SKBR-3 cells in a dose dependent manner. This binding was detected on FACS using a FITC-conjugated secondary antibody against Herceptin. Secondary antibody detection of primary binding events is a common technique used for FACS analysis and has been shown to have greater sensitivity than directly labeling the primary antibody.³⁵

The binding assay was performed at 4 °C to inhibit cellular internalization of Herceptin immunonanoparticles.³⁶ By excluding cellular uptake, cellular interactions included only binding and dissociation events, thereby allowing the measurement of the equilibrium binding isotherm. Importantly, surface bound immunonanoparticles were accessible to the secondary antibody used in the FACS analysis and thus did not require permeabilization of the cell membrane for detection. Because the fluorescence intensity is proportional to the number of immunonanoparticles bound to cells, the binding constant K_{eq} and the saturation fluorescence intensity I^{MAX} can be fitted using the Langmuir model *via*:

$$I(C_{NP}) = \frac{I^{MAX} K_{eq} C_{NP}}{1 + K_{eq} C_{NP}} \quad (11)$$

where $I(C_{NP})$ is the concentration-dependent measured fluorescence intensity. The fractional coverage, θ , can then be calculated by dividing the measured fluorescence intensity by the saturation

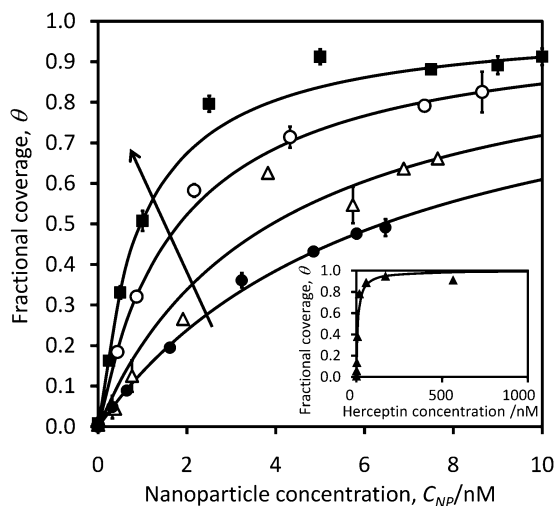


Fig. 2 Fractional coverage of Herceptin immunonanoparticles bound to HER2 overexpressing SKBR-3 cells as a function of immunonanoparticle concentration. The arrow indicates ascending order of antibody conjugation density: Herceptin immunonanoparticles bearing 1.9 (●), 3.2 (△), 5.9 (○), and 9.4 (■) antibodies; inset shows fractional coverage for free Herceptin (▲).

fluorescence intensity. The equilibrium binding of single Herceptin antibodies and Herceptin immunonanoparticles to SKBR-3 cells closely follow the Langmuir isotherms indicated by the solid lines (see Fig. 2). The R^2 value for each fitted line exceeds 0.95.

The fitted K_{eq} values increase linearly with the antibody conjugation density from 0.11 nM^{-1} for single Herceptin antibodies (which are likely similar to those that would be obtained from immunonanoparticles bearing 1.0 antibody per particle) to 1.03 nM^{-1} for the immunonanoparticles bearing 9.4 antibodies per particle (Fig. 3A). This 10-fold increase in K_{eq} corresponds to a nearly 10-fold increase in the number of antibodies available per immunonanoparticle. These variations agree well with the model for monovalent binding behaviour, described by Equation 9, where the cell-particle affinity increases due to an amplified number of unique binding states. Likewise, the variations in $\Delta\bar{G}$ (Fig. 3B) are in remarkable agreement with logarithmic scaling (see Equation 10), where a fitted proportionality constant ($1.01RT$) is within 1% of the theoretical value (RT) obtained, along with a $\Delta\bar{G}(1)$ of -51.5 kJ/mol . No threshold antibody

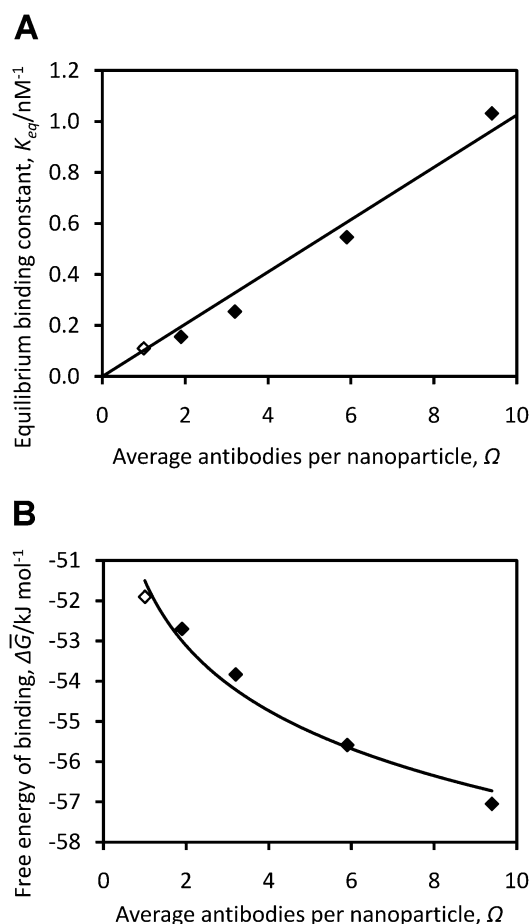


Fig. 3 (A) K_{eq} and (B) $\Delta\bar{G}$ increase in absolute value as the number of Herceptin antibodies per nanoparticle increases, thereby indicating greater binding affinity. The open symbols (\diamond) represent the values calculated for free Herceptin, which denotes a monovalent case, and the closed symbols (\blacklozenge) represent Herceptin immunonanoparticles. The trends in (A) and (B) follow the theoretical behaviour of monovalent immunonanoparticle binding.

density for binding was observed, which is consistent with previous reports on targeted particles having flexible spacers between the targeting molecule and the core.^{32,37,38} This immunonanoparticle approach yields the flexibility to use a particular IgG antibody for a targeting application with K_{eq} up to an order of magnitude greater than its original value in a tunable manner.

The variations in K_{eq} and $\Delta\bar{G}$ do not support the occurrence of multivalent binding, which is predicted to give rise to a much more dramatic, near-exponential increase in K_{eq} and a near-linear increase in $\Delta\bar{G}$ in the case where all antibodies on a bound immunonanoparticle participate in binding ($\alpha = \Omega$, see Equations 3 and 4). Even in the case where only a fraction of antibodies are bound ($\alpha < \Omega$), if they occur with great enough frequency to influence the average system behaviour, the increased binding valency should strengthen binding over the predicted values for increased binding configurations given by the monovalent binding model. Instead, the monovalent binding model accurately described the magnitude of the increases in K_{eq} without the need to account for contributions due to multivalent interactions. These findings support the increase in the number of possible binding configurations associated with monovalent binding as the main driver of the enhanced binding strength.

These observations are consistent with the small fraction of the nanoparticle surface that comes in contact with the cell upon binding. Herceptin is an IgG class antibody, an isotype which occupies an area with a 30 nm diameter.³⁹ The 80 nm immunonanoparticles tested are highly curved compared to the cell surfaces and likely give rise to a small cell-particle contact area; the small contact area compared to the area occupied by each antibody makes it improbable for multiple antibodies to be localized at the cell-particle interface, even with the antibody mobility provided by the flexible PEG spacer as an attachment point to the particle core. Hence, the amplified binding of nanoparticles targeted using large targeting molecules (*e.g.*, whole antibodies or antibody fragments)^{40,41} is likely caused by an increase in the number of monovalent binding states, and not the multivalent interactions to which it has formerly been attributed. Nanoparticles that are densely covered with smaller targeting ligands (*e.g.*, hundreds or thousands of low molecular weight molecules per particle)^{9,19,38,42} may still exhibit multivalent cell-particle interactions, which, unlike the system described here, can lead to a non-linear K_{eq} versus Ω dependence.

The agreement between the data in Fig. 3 and monovalent binding model suggests that immunonanoparticle binding strength can be predictably tuned by adjusting the number of conjugated Herceptin antibodies according to Equation 9. This agreement between the predicted fractional coverage (calculated from the fitted $\Delta\bar{G}(1)$ -value) and that obtained experimentally using either free Herceptin or the Herceptin immunonanoparticles is further illustrated in Fig. 4. The experimental θ values are closely correlated to the theoretical predictions ($R^2 = 0.99$), supporting Equation 9 as a useful quantitative guideline for designing immunonanoparticles for targeted drug delivery to tumour sites.

Looking forward, quantification of the binding isotherm also guides *in vivo* dosage requirements by expressing the intratumoural particle concentration required to reach a desired fraction of saturation binding. Approaching saturating particle levels maximizes receptor binding as a gateway to receptor

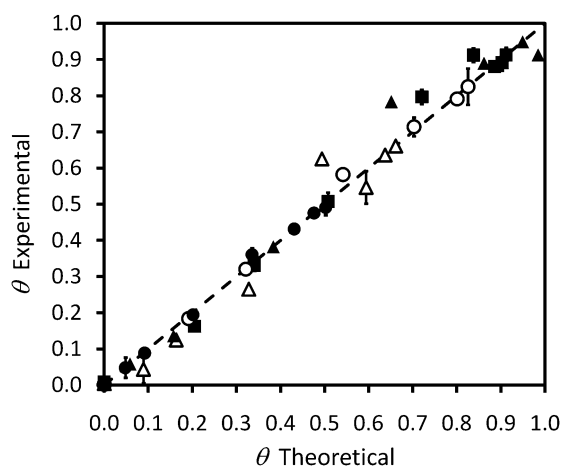


Fig. 4 Comparison of the experimental and theoretical fractional coverages (θ) of SKBR-3 cells by free Herceptin (\blacktriangle) and Herceptin immunonanoparticles bearing 1.9 (\circ), 3.2 (\triangle), 5.9 (\circ), and 9.4 (\blacksquare) antibodies exhibiting monovalent binding. The experimentally derived θ values closely match the theoretically predicted θ values, with $R^2 = 0.99$.

mediated cellular uptake, making this an important parameter for many targeted drug delivery strategies.¹⁸

Conclusions

The binding isotherms of Herceptin immunonanoparticles bound to HER2 overexpressing SKBR-3 cells were measured at varying levels of antibody conjugation using a flow cytometric immunoassay, thereby quantifying binding strength using a direct live cell assay. Based on these measurements, a thermodynamic analysis of the binding valency was completed and the resulting valency of antibody-receptor binding interactions of immunonanoparticles bearing multiple targeting antibodies was investigated. Binding affinity increases with increasing antibody conjugation density in a manner consistent with the theory for monovalent binding, suggesting that multivalent interactions are not the primary cause of the amplified binding strength. The Herceptin immunonanoparticle formulations tested can be selected for values of K_{eq} up to an order of magnitude greater than the value for free Herceptin. This method can also be applied to other particle formulations having multiple targeting ligands to better understand how the number of ligands affects the binding valency of a particular system, and how this property can then be manipulated to control effective binding affinity. The resulting understanding of the mechanism governing the increase in binding strength can be used in a predictive manner to guide nanoparticle design.

Acknowledgements

We thank Simone Helke for her advice and technical support in developing our methods for analysis of antibody binding using FACS. We are grateful to the Natural Sciences and Engineering Research Council and the Canadian Institutes for Health Research for funding through the Collaborative Health Research Program.

References

- R. Cairns, I. Papandreou and N. Denko, *Mol. Cancer Res.*, 2006, **4**, 61–70.
- K. J. Cho, X. Wang, S. M. Nie, Z. Chen and D. M. Shin, *Clin. Cancer Res.*, 2008, **14**, 1310–1316.
- F. Marcucci and F. Lefoulon, *Drug Discov. Today*, 2004, **9**, 219–228.
- P. A. Trail, H. D. King and G. M. Dubowchik, *Cancer Immunol. Immun.*, 2003, **52**, 328–337.
- J. W. Park, D. B. Kirpotin, K. Hong, R. Shalaby, Y. Shao, U. B. Nielsen, J. D. Marks, D. Papahadjopoulos and C. C. Benz, *J. Control. Release*, 2001, **74**, 95–113.
- M. Shi, J. H. Wosnick, K. Ho, A. Keating and M. S. Shoichet, *Angew. Chem. Int. Ed.*, 2007, **46**, 6126–6131.
- G. P. Adams, R. Schier, A. M. McCall, H. H. Simmons, E. M. Horak, R. K. Alpaugh, J. D. Marks and L. M. Weiner, *Cancer Res.*, 2001, **61**, 4750–4755.
- Y. Zhou, C. Daryl, H. Zou, M. E. Hayes, G. P. Adams, D. B. Kirpotin and J. D. Marks, *J. Mol. Biol.*, 2007, **371**, 934–947.
- D. W. Bartlett and M. E. Davis, *Bioconjugate Chem.*, 2007, **18**, 456–468.
- J. Panyam and V. Labhasetwar, *Adv. Drug Deliver. Rev.*, 2003, **55**, 329–347.
- L. Nobs, F. Buchegger, R. Gurny and E. Allemann, *J. Pharm. Sci.-US*, 2004, **93**, 1980–1992.
- C. A. Janeway, P. Travers, M. Walport and M. J. Shlomchik, *Immunobiology: the immune system in health and disease*, 6 edn., Garland Science, New York, 2005.
- L. L. Kiessling, J. E. Gestwicki and L. E. Strong, *Current Opinion in Chemical Biology*, 2000, **4**, 696–703.
- G. P. Adams, R. Schier, K. Marshall, E. J. Wolf, A. M. McCall, J. D. Marks and L. M. Weiner, *Cancer Res.*, 1998, **58**, 485–490.
- S. Kubetzko, E. Balic, R. Waibel, U. Zangemeister-Wittke and A. Pluckthun, *J. Biol. Chem.*, 2006, **281**, 35186–35201.
- R. A. Beckman, L. M. Weiner and H. M. Davis, *Cancer*, 2007, **109**, 170–179.
- M. Juweid, R. Neumann, C. Paik, M. J. Perezbacete, J. Sato, W. Vanosdol and J. N. Weinstein, *Cancer Res.*, 1992, **52**, 5144–5153.
- C. M. Paulos, J. A. Reddy, C. P. Leamon, M. J. Turk and P. S. Low, *Molecular Pharmacology*, 2004, **66**, 1406–1414.
- S. Hong, P. R. Leroueil, I. J. Majoros, B. G. Orr, J. R. Baker and M. M. B. Holl, *Chem. Biol.*, 2007, **14**, 105–113.
- C. Zahnd, F. Pecorari, N. Straumann, E. Wyler and A. Pluckthun, *J. Biol. Chem.*, 2006, **281**, 35167–35175.
- T. Soukka, H. Harma, J. Paukkunen and T. Lovgren, *Anal. Chem.*, 2001, **73**, 2254–2260.
- H. D. Zhang, P. S. Williams, M. Zborowski and J. J. Chalmers, *Biotechnology and Bioengineering*, 2006, **95**, 812–829.
- J. Y. Wong, T. L. Kuhl, J. N. Israelachvili, N. Mullah and S. Zalipsky, *Science*, 1997, **275**, 820–822.
- C. L. Arteaga, *Breast Cancer Res.*, 2003, **5**, 96–100.
- J. Baselga and J. Albanell, *Ann. Oncol.*, 2001, **12**, 35–41.
- W. E. Carson, R. Parihar, M. J. Lindemann, N. Personeni, J. Dierksheide, N. J. Meropol, J. Baselga and M. A. Caligiuri, *Eur. J. Immunol.*, 2001, **31**, 3016–3025.
- D. J. Slamon, G. M. Clark, S. G. Wong, W. J. Levin, A. Ullrich and W. L. McGuire, *Science*, 1987, **235**, 177–182.
- U. B. Nielsen, D. B. Kirpotin, E. M. Pickering, D. C. Drummond and J. D. Marks, *BMC Immunol.*, 2006, **7**, 24.
- M. Shi and M. S. Shoichet, *Journal of Biomaterials Science: Polymer Edition*, 2008, **19**, 1143–1157.
- U. B. Nielsen, G. P. Adams, L. M. Weiner and J. D. Marks, *Cancer Res.*, 2000, **60**, 6434–6440.
- Y. Stupp, T. Yoshida and W. E. Paul, *J. Immunol.*, 1969, **103**, 625–627.
- A. Gabizon, A. T. Horowitz, D. Goren, D. Tzemach, F. Mandelbaum-Shavit, M. M. Qazen and S. Zalipsky, *Bioconjugate Chem.*, 1999, **10**, 289–298.
- M. Mammen, S. K. Choi and G. M. Whitesides, *Angew. Chem. Int. Ed.*, 1998, **37**, 2755–2794.
- H. T. Davis, *Statistical Mechanics of Phases, Interfaces and Thin Films*, VCH Publishers, Inc., New York, 1996.
- S. Y. Mao, *Methods Mol. Biol.*, 1999, **115**, 35–38.

-
- 36 T. Seddiki and M. Ollivierbousquet, *European Journal of Cell Biology*, 1991, **55**, 60–70.
- 37 R. J. Lee and P. S. Low, *Biochimica Et Biophysica Acta-Biomembranes*, 1995, **1233**, 134–144.
- 38 R. J. Lee and P. S. Low, *Journal of Liposome Research*, 1997, **7**, 455–466.
- 39 C. J. Roberts, P. M. Williams, J. Davies, A. C. Dawkes, J. Sefton, J. C. Edwards, A. G. Haymes, C. Bestwick, M. C. Davies and S. J. B. Tendler, *Langmuir*, 1995, **11**, 1822–1826.
- 40 S. Muro, T. Dziubla, W. N. Qiu, J. Leferovich, X. Cui, E. Berk and V. R. Muzykantov, *Journal of Pharmacology and Experimental Therapeutics*, 2006, **317**, 1161–1169.
- 41 J. Willuda, S. Kubetzko, R. Waibel, P. A. Schubiger, U. Zangemeister-Wittke and A. Pluckthun, *J. Biol. Chem.*, 2001, **276**, 14385–14392.
- 42 R. Weissleder, K. Kelly, E. Y. Sun, T. Shtatland and L. Josephson, *Nature Biotechnology*, 2005, **23**, 1418–1423.